Prediction and validation of intermetallic compound formation during friction stir welding of AA6061 to commercially pure copper

Gihad Karrar*[1], Alexander Galloway[1], Athanasios Toumpis[1], Fadi Al-Badour[2], Hongjun Li[3]

[1]Department of Mechanical & Aerospace Engineering, University of Strathclyde, Glasgow G1 1XJ, U.K.

[2]Mechanical Engineering Department, King Fahd University of Petroleum and Minerals, Dharan, 31261, Saudi Arabia.

[3]Faculty of Mechanical Engineering and Automation, Zhejiang Sci-Tech University, Xiasha Higher Education Zone, Hangzhou 310018, China.

*Corresponding author, gihad-mohamed-karrar-babekr@strath.ac.uk

Abstract

A novel approach for predicting the intermetallic compound formation during friction stir welding of AA6061 to commercially pure copper has been developed, in addition to their effect on mechanical properties. The temperature distribution of the aluminium to copper weld nugget determined by a finite element model, the use of an Al-Cu phase diagram and the elemental concentration of copper and aluminium in the weld nugget have been combined to predict and validate several intermetallic compounds present in the different zones of the weldment. The results of performing butt-welding of these dissimilar metals using the friction stir welding process demonstrated that the highest ultimate tensile strength of 194.5 MPa was achieved at 1500 rpm tool rotational speed, 100 mm/min traverse speed and a zero-tool offset.

Keywords Intermetallic compounds; Friction stir welding; Joint integrity; Dissimilar joining; Modelling; Metallurgy

1. Introduction

There are advantages in partially replacing copper with aluminium for certain engineering applications such as electrical connectors, tubes of heat exchangers, transformer foil conductors and capacitor foil windings [1-2]. This is largely driven by the similarities in the electrical properties of each metal. Beyond this, the reduced cost and the lower mass of aluminium renders it an attractive partial substitute for

This is a peer-reviewed, accepted author manuscript of the following article: Karrar, G., Galloway, A., Toumpis, A., Al-Badour, F., & Li, H. (Accepted/In press). Prediction and validation of intermetallic compound formation during friction stir welding of AA6061 to commercially pure copper. Science and Technology of Welding and Joining.

copper [3]. In circumstances where there is a need to weld the substitute aluminium part to pure copper, significant challenges emerge as a result of the differences in the physical, thermal and mechanical properties of each metal. Based on the relative advantages against conventional fusion welding processes, i.e. absence of porosity, solidification cracking, oxidation and lower distortion, the friction stir welding (FSW) technique can replace the conventional joining methods due to the ability of FSW to weld dissimilar metals and alloys that are defect-free and exhibit better joint quality [4].

Nevertheless, challenges arise when joining aluminium to copper using FSW, particularly the formation of intermetallic compounds (IMCs) at the interface zone and weld nugget. There have been some attempts to predict and control the formation of IMCs in dissimilar friction stir welds; Mishra et al. [5] proposed the first approach for predicting the IMCs in such cases. By assuming a simple material volume under the FSW tool, they [5] qualitatively showed that, with the aid of a phase diagram, IMC formation can be predicted if the tool offset is carefully controlled. However, as their approach [5] took no account of the thermo-mechanical effect during the FSW process, the ability to accurately predict the IMC formation is questioned [2]. Additionally, the material volume beneath the FSW tool is known to form a simple parallelepiped shape which was not accounted for in their [5] work. More recently, Shailesh et al. [6] advanced the work of Mishra et al. [5] by assuming a cylindrical material volume under the FSW tool. Although the derived equations of Shailesh et al. [6] were valid and logically accepted to represent the material volume under the FSW tool, there was again an absence of accurate thermo-mechanical data to fully support their method.

In addition to the above predictive approaches, some attempts have been performed to understand the formation of these IMCs as well as their effect on the joint mechanical properties. Ouyang et al. [7] studied the microstructural evolution during FSW of AA6061-T6 to copper, where the dissimilar weld nugget exhibited several IMCs such as Al_2Cu, AlCu and Al_4Cu_9. In their work [7], thermocouples were located at 2 mm, 4 mm, and 6 mm from the pin area and towards the aluminium (the retreating side). It was found [7] that the measured temperature of the AA6061 reached 580°C, which is greater than the melting temperature at the eutectic composition of an Al-Cu binary alloy. The authors [7] proposed that these IMCs

evolved on the basis of two different phenomena, these being (a) the constitutional liquation that governs the formation of aluminium-rich phases (Al/Al_2Cu eutectics, Al_2Cu and AlCu), which is due to their solidified morphology, and (b) their relatively lower melting temperature. In contrast, the solid-state diffusion phenomenon was claimed to control the formation of the copper-rich intermetallic structures in the weld zone (Cu(Al) and Al_4Cu_9). This can be attributed to the thermo-mechanical effect of FSW at the weld nugget, where the melting temperature of Al_4Cu_9 (1030°C) is higher than the peak temperature during FSW. It was concluded [7] that the existence of these brittle IMCs created a high level of disparity in the mechanical properties of the weld. In their work [7], there was an absence of the resultant high strain rate effect in the evolution of the relatively lower melting temperature IMCs (Al_2Cu and AlCu), as the thermo-mechanical effect of FSW can also explain the formation of these IMCs.

More recently, Galvao et al. [8] claimed that the IMC formation in dissimilar FSW of aluminium to copper can only be explained by the thermo-mechanically activated solid state diffusion phenomenon. Unlike the approach of Ouyang et al. [7], Galvao et al. [8] proved the absence of solidification structures in both the aluminium and copper rich sides and reported that the resultant high strain rate during the FSW process facilitates the formation of Al_2Cu, AlCu and Al_4Cu_9, an approach that has also been supported in other recent publications [9-11]. Further, Xue et al. [12] and Galvao et al. [13] investigated the influence of process parameters on the evolution of IMCs during FSW of aluminium to copper. They claimed that the location of each material with respect to the advancing side (AS) of the FSW tool, as well as the tool rotational speed relative to the welding speed (ω/v), have a significant effect on the IMC formation and subsequently the joint mechanical strength. Other published work [14-15] demonstrated that a thin continuous IMC layer in aluminium to copper could significantly improve the mechanical properties of the joint in which the predominant IMCs in the weld nugget were Al_2Cu and Al_4Cu_9 and that their presence resulted in a tensile strength equating to 80% of the aluminium base alloy.

Overall, researchers [3-15] have not definitively demonstrated the negative or positive role played by the IMC particles. Furthermore, there is a lack of understanding towards the evolution of these IMCs during the FSW process of aluminium to copper. Additionally, there is a clear lack of reporting on the quantitative nature of the IMCs in the weld nugget.

The primary purpose behind the current study is to achieve better and consistent weld quality by controlling the IMC formation. Furthermore, as it is expected that IMC formation during FSW is intrinsically based on a thermo-mechanical phenomenon governed by the combined effect of temperature, plastic deformation, and material mixing, it is clear that the prediction of any evolved IMCs during FSW of aluminium to copper must be based on accurate numerical thermo-mechanical data combined with phase diagram information.

Hence, the current systematic study presents a highly novel approach for accurately predicting the IMC formation in FSW of dissimilar AA6061 to copper based on three related criteria as follows; (1) the thermal outputs from the finite element model developed by Al-Badour et al. [16], (2) the use of the Al-Cu phase diagram to identify the evolved IMCs as a function of the thermal outputs and (3) a robust microstructure and property evaluation to validate the IMC formation predicted from criteria (1) and (2), allowing the mechanical properties of the joint to be determined as a function of the type of IMCs that are formed.

2. Methodology

2.1. Numerical model development

A coupled Eulerian Lagrangian (CEL) model [16] is applied to simulate the FSW process of joining AA6061 to copper. For the multilayers of complexity to formulate the problem, CEL is the most appropriate modelling solution [19-21]. CEL captures the severe plastic deformation by avoiding the distortion of the mesh during the process, where the material flows through a stationary mesh in the Eulerian domain. The Abaqus Explicit Solver environment is used to implement and solve the model.

A geometrical model of 300 x 50 x 3 mm^3 (Eulerian domain) is assumed with three distinctive areas in this domain; the copper plate (retreating side (RS)), the aluminium plate (AS) and a void layer of 1 mm in thickness to visualise the flash formation during the process. A simple, featureless FSW tool pin of 4.5 mm diameter and shoulder of 18 mm diameter are considered as a Lagrangian rigid body domain; thus, all the physical properties and boundary steps are assigned to a unique reference point.

A fine biased seeding mesh is considered along and around the FSW shoulder area (region of high plastic deformation), where the mesh becomes coarser towards the Eulerian domain sides. Multi-layer thermally coupled elements are assumed for the Eulerian plates.

Unlike the CEL model reported by Al-Badour et al. [16], the FSW tool herein is assumed to rotate and traverse along the Eulerian domain, while this domain is only constrained against the velocities and displacements on its sides. Fig. 1 (a) shows the typical boundary conditions for Eulerian and Lagrangian domains as well as the dissimilar materials placement where Fig. 1 (b) illustrates the finer mesh within the shoulder area. The initial temperature for all the model parts is assumed to be uniform and equal to 25°C.

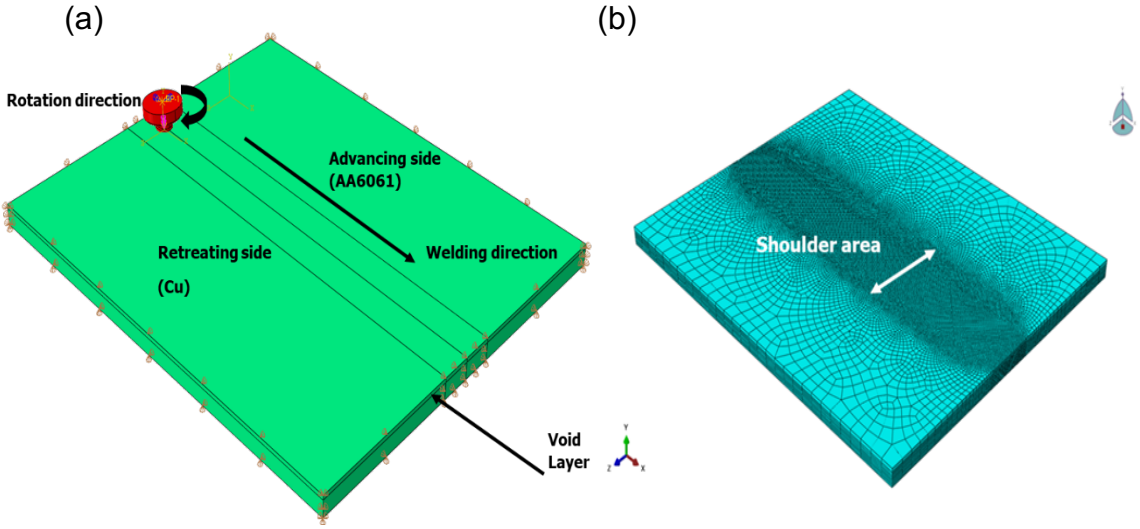

Fig. 1. (a) Applied boundary conditions and placement of each material. (b) Mesh in the vicinity of the FSW shoulder area.

2.1.1. Material properties

Due to plastic deformation in the FSW zone at high temperatures and strain rates, the Johnson-Cook's constitutive model [20], shown in Eq. (1), is considered to formulate the plasticity of the dissimilar materials. Thus, the material flow/yield stress σ_0 is described as a function of plastic strain, strain rate and temperature.

$$\sigma_0 = [A + B\varepsilon_{pl}^{n}].[1 + C\ln\frac{\dot{\varepsilon_{pl}}}{\dot{\varepsilon_0}}].\ [1 - \left(\frac{T - T_{ref}}{T_{melt} - T_{ref}}\right)^{m}] \quad (1)$$

$* \ T_{ref} \leq \mathrm{T} \leq \ T_{melt}$

Where A is the yield stress at a reference strain rate and temperature (MPa), B is the coefficient of strain (MPa), C and m are the Johnson-Cook's model parameters that represent the coefficient of strain rate sensitivity and thermal softening exponent, and n is the strain hardening exponent. Table 1 presents these material constants for both AA6061 and copper at a reference temperature (room temperature T_{ref}, T_{melt} is the material solidus temperature, ε_{pl}^{n}, $\dot{\varepsilon_{pl}}$ and $\dot{\varepsilon_0}$ are the effective plastic strain, effective plastic strain rate and normalising strain rate, respectively.

Other material properties, such as density, thermal expansion coefficient, specific heat capacity, Poisson's ratio and modulus of elasticity, are considered as temperature dependent. Tables 2 and 3 summarise the variation of material properties of AA6061 and copper with temperature, up to the melting point of both AA6061 and copper.

Table 1

Johnson-Cook's parameters [23]

Material	A (MPa)	B (MPa)	C	n	m	$T_{ref.}$ (°C)	$T_{melt.}$ (°C)
AA6061	324	114	0.002	0.42	1.09	25	582
Copper	90	292	0.025	0.31	1.09	25	1083

Table 2

Temperature dependent material properties of AA6061 in the range of 25°C– 482°C

Temperature (°C)	Specific heat ($J\ kg^{-1}\ °C^{-1}$)	Thermal conductivity ($W\ m^{-1}\ °C^{-1}$)	Young's modulus (GPa)	Density ($kg\ m^{-3}$)	Coefficient of thermal expansion (10^{-6}) (°C)
25	870	140	66.94	2690	23.4
100	920	168	63.21	2690	24.6
200	960	183	56.8	2660	26.6
250	1000	196	52.0	2645	27.5

300	1040	208	47.17	2630	28.5
400	1150	219	32.67	2600	29.5
482	1280	220	20.2	2600	30.5

Table 3

Temperature dependent material properties of copper in the range of 25°C – 1060°C

Temperature (°C)	Specific heat ($J\ kg^{-1}\ °C^{-1}$)	Thermal conductivity ($W\ m^{-1}\ °C^{-1}$)	Young's modulus (GPa)	Density ($kg\ m^{-3}$)	Coefficient of thermal expansion (10^{-6}) (°C)
25	384.60	398	117.2	8940	16.7
100	393.4	390	114.42	8940	17.3
200	405.13	387.3	110.32	8940	18.3
250	411.00	386	107.56	8940	18.6
350	416.00	383	99.98	8940	19.2
530	431.98	371	96.95	8940	20.4
630	440.67	364	93.25	8940	21.4
730	448.62	357	90.20	8940	22.4
930	468.14	343	87.33	8940	24.8
1060	476.19	334	84.75	8940	26.36

2.1.2. Friction coefficient

Defining the contact condition between the FSW tool and the dissimilar materials is complex to formulate. Assuming sticking boundary conditions [21], the coefficient of friction as a function of pressure and slip rate [22] or Coulomb's law [16] are the main approaches to simulate the interaction condition between the FSW tool and the workpiece. In the present work, the modified friction law described by Shokri et al.

[23] is considered to couple the interaction between the Lagrangian (tool) and Eulerian (aluminium and copper) domains, while both sticking and slipping conditions can be involved. An intermediate value of τ_{max} is chosen where, above this value, the sliding conditions are no longer applicable, i.e., $\tau_{max} \neq \mu \times P_{contact}$, μ and $P_{contact}$ are the coefficient of friction and contact pressure, respectively. The τ_{max} value is calculated from the Von-Mises relationship in Eq. (2) by considering that:

$$\tau_{max} = \tau_u = \alpha\left(\frac{\sigma_{u,Al}+\sigma_{u,Cu}}{\sqrt{3}}\right) \quad (2)$$

Where $\tau_u \; and \; \sigma_u$ are the ultimate shear stress and ultimate material strength and α is the material volume fraction, equal to 0.5 at the joint line. An average value of 0.5 for the friction coefficient μ is assumed for the interaction between aluminium, copper and steel (FSW tool) during the sticking condition where no voids are formed.

2.2. Experimental methodology

2.2.1. Materials and FSW process details

A fully instrumented HT-JM16X8/2 static gantry FSW machine was employed to butt weld 300 x 50 x 3 mm³ thick commercially pure copper and AA6061 plates along their lengths. A high strength steel FSW tool with a featureless tool pin design was used in the experiments. The tool pin diameter (Dp) and length (plunging depth, Pd) was 4.5 mm and 2.7 mm, respectively, while the shoulder diameter (Ds) was 18 mm. The nominal chemical composition and mechanical properties of the two parent materials are presented in Tables 4 and 5, respectively. Defect-free joints were obtained when positioning the soft material (AA6061) on the AS with 0 mm tool offset, therefore, the main purpose of this work was to predict and validate the IMC evolution under this material placement configuration. The welds were performed at different ω/v ratios and at a constant tool welding speed of 100 mm/min. All FSW parameters are shown in Table 6. A schematic illustration of the experimental set up is shown in Fig. 2 (a).

The temperatures in the weld zone were measured by K-type thermocouples embedded at different positions (11-13 mm) from the joint line, i.e., 2- 4 mm from the shoulder surface. A series of holes (1.5 mm in diameter) were drilled from the side of AA6061 (As) and the side of copper (Rs), as shown in Fig. 2 (b). These holes were located at the mid-region (i.e., 150 mm from the starting point) of the plate length to

allow for steady state FSW conditions to be developed. Fig. 3 (a) and (b) show a transverse cross-section and a top view of the relative location of the FSW tool at 0 mm and d mm tool offset, respectively.

Table 4

Chemical composition (in wt.%) of AA6061 and commercially pure copper

AA6061 (wt. %)	**Si**	**Mg**	**Cu**	**Mn**	**Zn**	**Cr**	**Fe**
	0.6	1.0	0.3	0.15	0.25	0.10	0.7
Copper (wt. %)	**Ag**	**Fe**	**Bi**	**Sb**	**As**	**Pb**	**S**
	0.035	0.05	0.001	0.002	0.002	0.005	0.005

Table 5

Mechanical properties of base metals

Materials	**Yield strength (MPa)**	**UTS (MPa)**	**EL (%)**	**Avg. HV**
AA6061	276	310	68.90	105
Copper	257.26	273.66	114.14	90

Table 6

Welding parameters used in the experiments

Condition Test no.	**ω/v ratio (rev/mm) ***	**Rotational Speed (rpm)**	**Backward tilt Angle (deg.)**	**Tool Offset, do (mm)**	**AS Material**
1	13	1300	2.8	0	AA6061
2	14	1400	2.8	0	AA6061
3	15	1500	2.8	0	AA6061

*The welding speed was maintained constant at 100 mm/min.

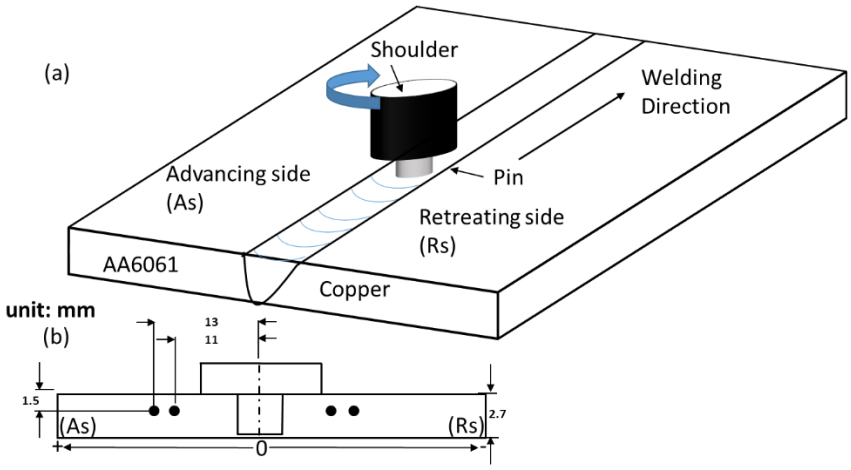

Fig. 2. (a) Weld configuration and experimental set-up (300 x 50 x 3 mm³). (b) The measurement positions of thermocouples imbedded into AA6061 (As) and copper (Rs).

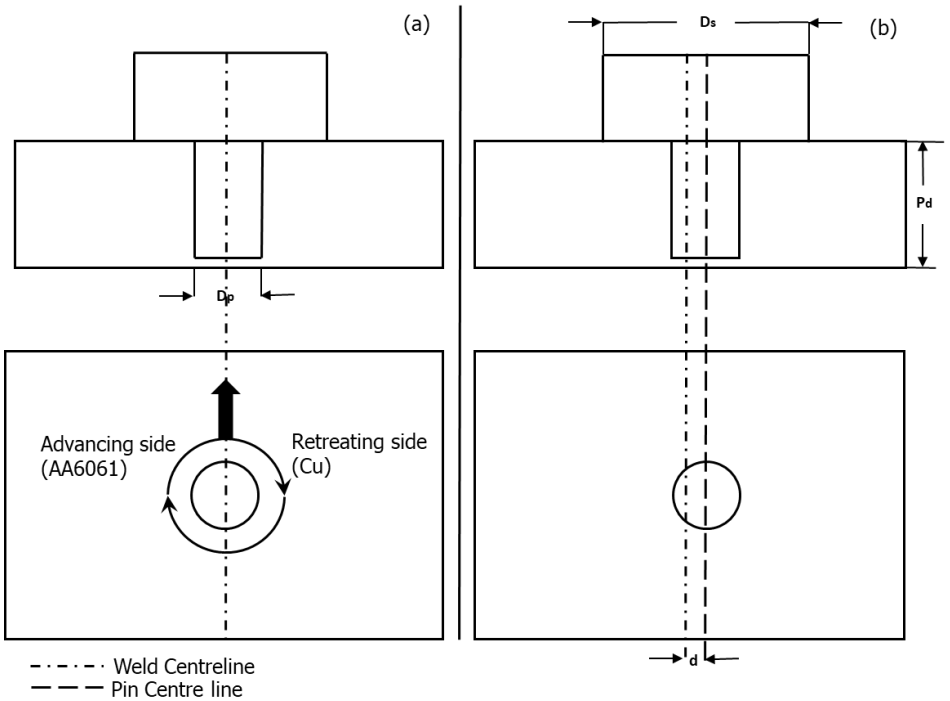

Fig. 3. (a) Transverse and top view showing the symmetrical location of the FSW tool at 0 mm tool offset. (b) The location at d mm tool offset.

2.2.2. Metallographic examination

Harvested samples from each weld zone were prepared using standard metallographic techniques. Etching was performed using a solution of 1 g of $FeCl_3$, 10 ml HCl, and 100 ml distilled water to first reveal the copper side, following which the AA6061 side was etched with a 12 s step using Weck's tint (4 g of $KMnO_4$ and 1 g of NaOH dissolved in 100 mL of distilled water). Thereafter, each etched sample was examined with the aid of high-resolution optical microscopy. In terms of compositional analysis and phase identification, energy dispersive spectroscopy (EDS) and X-ray diffraction (XRD) were performed at various locations of the weld joint. XRD was performed with a 40-mA operating current, 40-Kv voltage and 1.5406-Å Cu Kα radiation. A scanning rate of 0.02 deg./step within the range of 20°< 2θ< 100° was used throughout. Subsequently, the Topas Rietveld XRD method was implemented to quantify the IMCs content, as confirmed by XRD.

2.2.3. Mechanical testing

The joint mechanical strength was evaluated by testing sub-size specimens across the weld zone of each welded sample in accordance with ASTM-E8 [24], details of which are shown in Fig. 4. An average of five tests was reported for each welding condition. The samples were tested at a constant crosshead displacement rate of 2 mm/min using an Electro Plus E10000 Instron testing machine. The technique of hardness mapping was also employed to establish the relationship between IMC formation and joint mechanical strength. The measurements were carried out at mid-depth of the cross-sectional surface of welds using a load of 300 g and a dwell time of 15 sec.

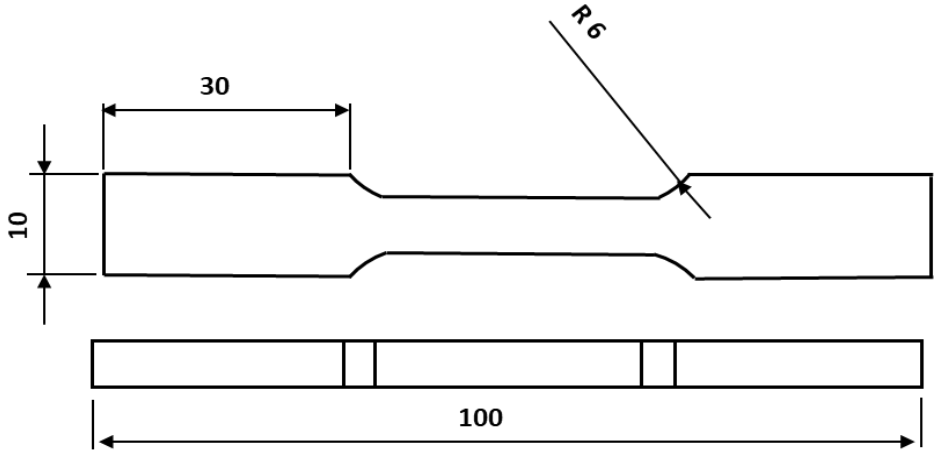

Fig. 4. Dimensions of the tensile sample as per ASTM E8 standard.

3. Results and discussion

3.1. Thermal model validation

Quantitatively, the nodal temperature history from the CEL model is compared to the experimental data at distances of 11 mm and 13 mm from the weld centreline, and towards both the AA6061 (AS) and copper (RS). To ensure a high degree of accuracy, care is taken by running the model exactly at the same welding parameters in test no. 2 (Table 6) of 1400 rpm, 100 mm/min and 0 mm tool offset. Fig. 5 (a) and (b) reveal the CEL model temperature history accompanied with the experimental temperature measurements recorded by thermocouples towards AS and RS, respectively. As shown from Fig. 5, the CEL with a modified friction law results in good agreement with the experimental data. It is also observed that the AS (AA6061) temperature is higher than the RS (copper) due to the fact that copper dissipated heat more rapidly than aluminium. This asymmetric behaviour of the temperature distribution was previously reported in a separate publication [12].

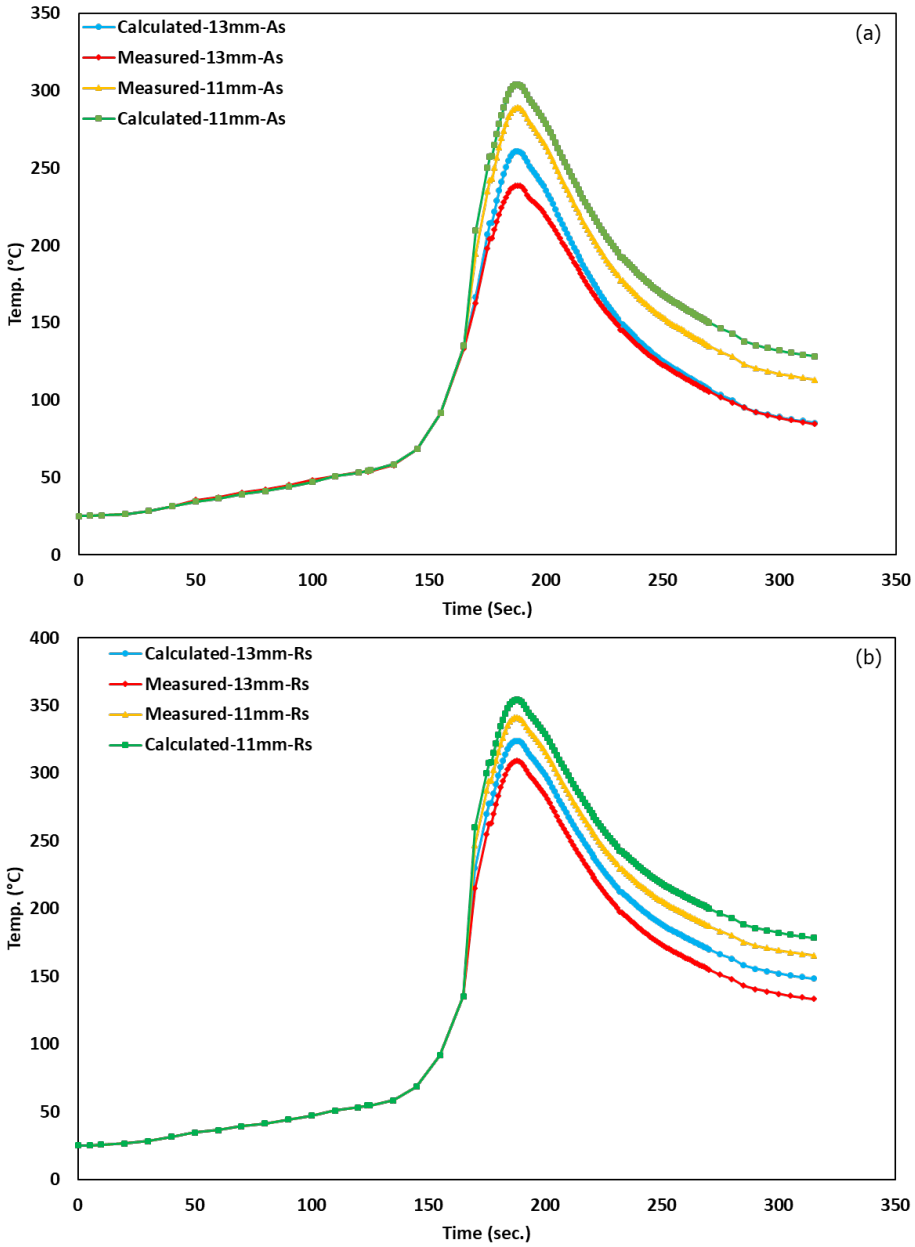

Fig. 5. Calculated vs measured temperature of 1400 rpm, 100 mm/min and 0 mm tool, at different positions from the pin centre toward both (a) the AS (AA6061) and (b) the RS (copper).

In the dissimilar FSW of aluminium to copper, the formation of IMCs is related to the welding parameters, i.e., frictional heat input (ω/v) ratio and tool offset. The formation of these IMCs greatly affects the joint quality in terms of mechanical strength, morphology, and defect formation [2, 5]. Thus, any attempts to control or inhibit the IMC evolution along the weld joint will significantly improve the joint quality. Hence, a qualitative analysis for the IMC formation based on the CEL model results together

with the Al-Cu binary system is presented. The effect of rotational speed (ω/v ratio), material placement, tool pin offset and the peak temperature are all considered in this analysis. The qualitative description for the IMC formation in FSW of aluminium to copper, based on the work of Shailesh et al. [6], has been modified and developed herein for use on aluminium to copper. Fig. 6 shows the material volumes of AA6061 and copper in the case of 0 mm tool offset (b), d mm tool offset (c). Where the total volume swept by the tool is given by Eq. (3), The volume of copper swept by the pin (V_{Cu}) can be expressed by Eq. (5), hence the ratio of copper swept volume over the total volume can be determined from Eq. (6).

$$V_{total} = \pi R_P^2 l \tag{3}$$

$$\cos\theta = \frac{d}{R_p} \tag{4}$$

$$V_{Cu} = \left\{R_P^2 \cos^{-1}\frac{d}{R_p} - d(R_P^2 - d^2)^{1/2}\right\} l \tag{5}$$

$$\frac{V_{Cu}}{V}(Cu.at\%) = \left\{\cos^{-1}\frac{d}{R_p} - d/R_P(1 - d^2/R_P^2)^{1/2}\right\}/\pi \tag{6}$$

* l ≡The cylindrical section height or length.

* R_P ≡The tool pin radius.

* V_{cu} ≡The swept copper volume by the FSW tool pin as per Fig. 6.

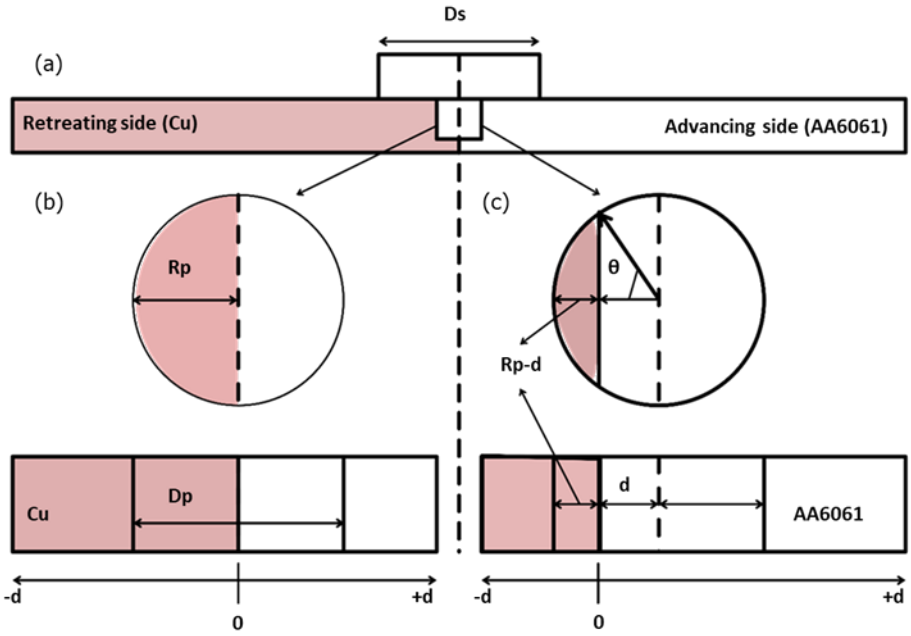

Fig. 6. Schematic of the material volume at different tool offsets.

Fig. 6 and Eq. 6 demonstrate that the tool offset affects the volume fraction of the total weld nugget, a prerequisite for IMC formation. Table 7, which summarises the predicted Al-Cu phases at different tool offsets towards both AA6061 and copper side, is constructed based on the Al-Cu equilibrium phase diagram, allowing the predicted phases to be determined based on the volume fraction of aluminium and copper (Fig. 7).

Table 7

Predicted phases at different tool offset

Tool offset	$d\ (mm)$	$at.\%\ Cu$	$at.\%\ AA6061$	Predicted Phases
0.5 mm towards AA6061	+0.5	35.97	64.03	Al_2Cu
1 mm towards AA6061	+1.0	10.96	89.04	Al(Cu)
0 mm offset	0	50.00	50.00	AlCu
0.5 mm towards Cu	-0.5	64.03	35.97	Al_4Cu_9
1.5 mm towards Cu	-1.5	89.04	10.96	Cu(Al)

The generic approach to control the IMC formation at the weld nugget is by positioning the tool in a way that keeps the compositions of aluminium to copper within the comfort zone, i.e., reduced possibility of IMC formation below the resulting temperature during FSW of AA6061 to copper [11]. Thus, the third aspect of this qualitative analysis is the temperature profile at the weld nugget. Fig. 8 (a) exhibits the top view of the temperature distribution at the welding stage in Kelvin at 0 mm tool offset. The same figure also shows that the peak temperature predicted by the CEL model is always lower than the aluminium melting temperature and within the plasticised zone. Fig. 8 (b) and (c) present cross-sectional views of the temperature profiles at 1400 rpm- 100 mm/min and 0 mm tool offset as well as 1500 rpm- 100 mm/min and 0 mm tool offset.

As observed, the calculated temperature within the weldment zone is affected by the tool rotational speed, where increasing the rotational speed increases the heat input and thus the temperature.

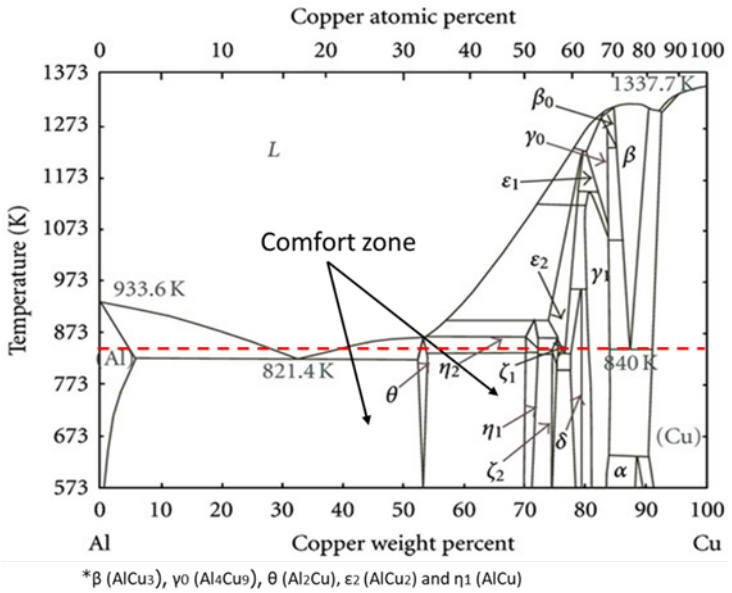

Fig. 7. Al-Cu equilibrium phase diagram (adapted from [25]).

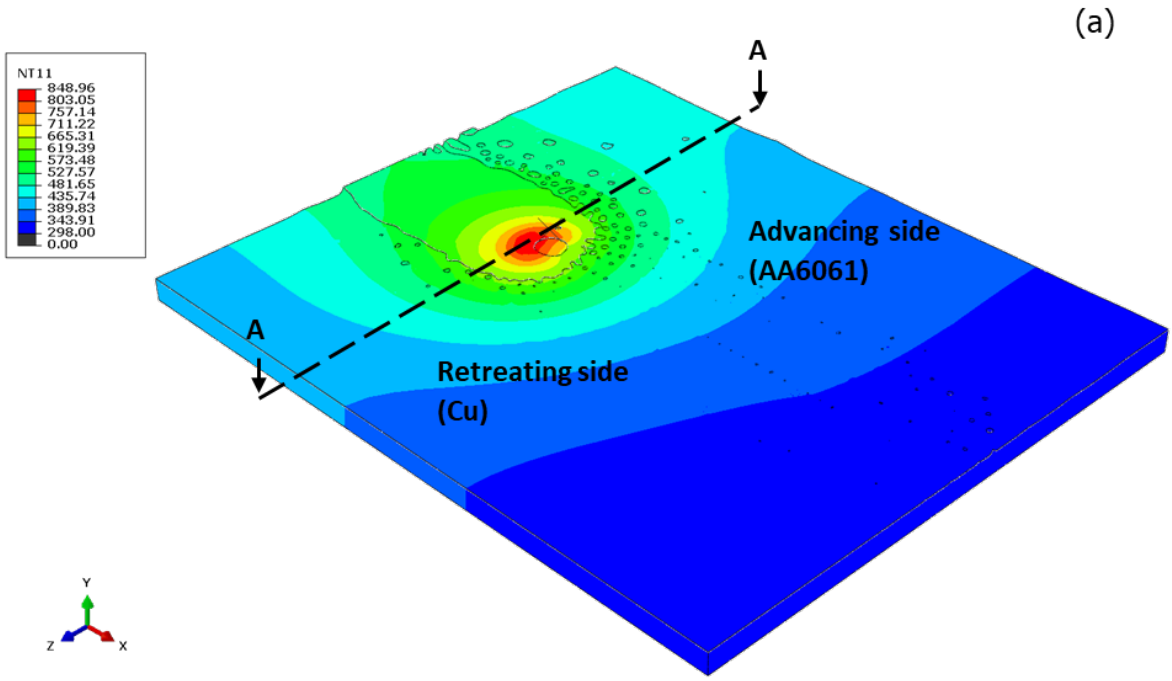

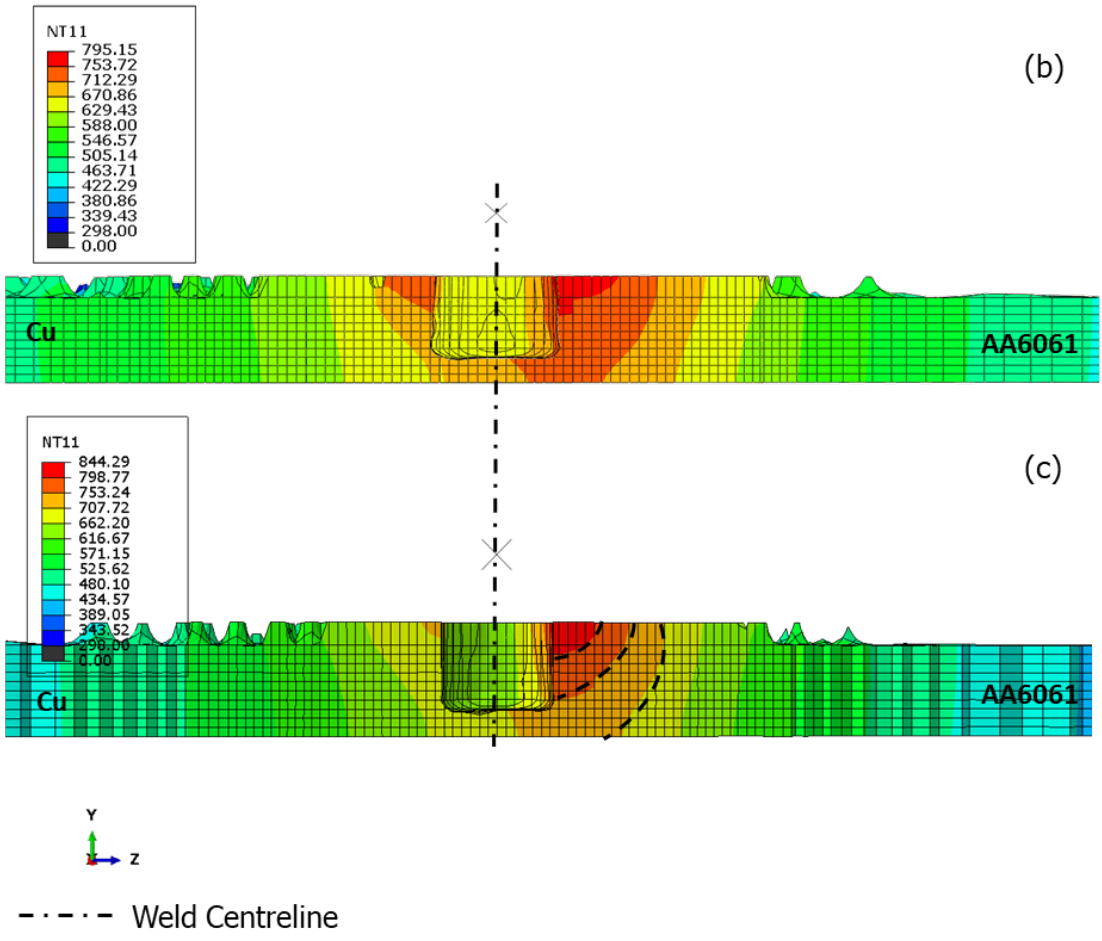

Fig. 8. (a) Top view of temperature profile at 1400 rpm and 100 mm/min, (b) cross-section view of temperature profile at 1400 rpm and 100 mm/min, (c) cross-section view of temperature profile at 1500 rpm and 100 mm/min.

3.2. Weld quality in the AA6061 - copper interface region

The weld quality of the AA6061-copper joint can be generally assessed when its cross-sectional macro features and microstructures are examined from the corresponding optical images. Fig. 9 (a) shows a macrograph of the dissimilar materials joint of test no. 1 at 1300 rpm rotational speed and 100 mm/min welding speed. Figs. 9 (b) and (c) show optical micrographs of the weldment at the interface region and the weld nugget, respectively. Close examination of Fig. 9 (c) reveals a degree of void formation at the weld nugget which is related to the irregular distribution of copper particles. Inadequate material flow, due to a suboptimal ω/v ratio, is the main reason for the resultant voids [1].

Fig. 9 (b) and Table 8 show the EDS analysis applied at different positions on the joint interface. The effective concentration of AlCu IMC was dominant with different Al/Cu contents in agreement with the calculations presented in section 3.1.

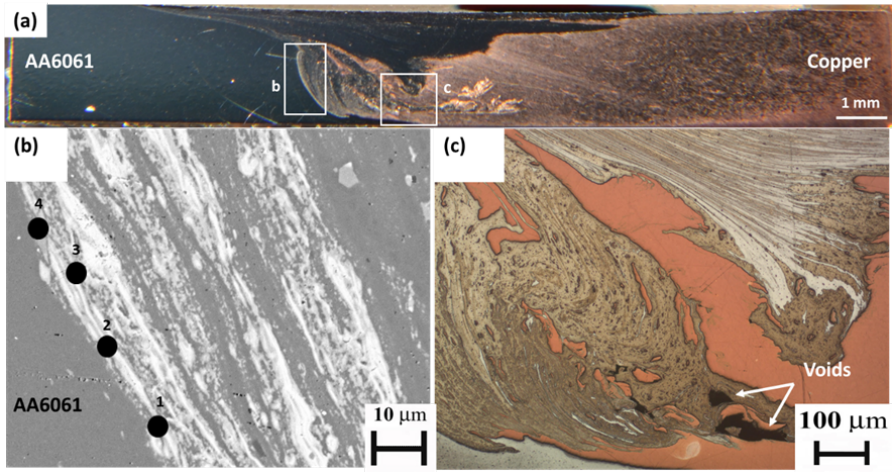

Fig. 9. (a) Typical cross-section of joint welded at 1300 rpm and 100 mm/min. (b) interface zone towards AA6061 side. (c) weld nugget.

Table 8

EDS results at weld nugget Test no. 1

Spectrum	Al at. %	Cu at. %	Probable Phase
1	55.27	44.73	AlCu
2	50.68	49.32	AlCu
3	62.62	37.38	Al_2Cu
4	33.72	66.28	Al_4Cu_9

Defect free joints were obtained at the higher rotational speeds of 1400 rpm and 1500 rpm (test nos. 2 and 3). Distinctive regions were observed across the weld joint. Towards the aluminium side (Fig. 10 (a & b)), relatively large copper particles were identified; these were irregularly distributed between the aluminium interface zone and the upper weld nugget surface. At the bottom of the aluminium interface zone, copper particles (fragments) were stretched and regularly distributed along the stir zone (SZ), as shown in Fig. 10 (c). Evidence of the intermixing between aluminium and copper particles was also observed at the weld nugget and towards

the copper side (Fig. 10 (d)). Unlike other researchers [7-8], placing the softer material (AA6061) on the AS with 0 mm tool offset resulted in defect free joints when a suitable ω/v ratio was selected.

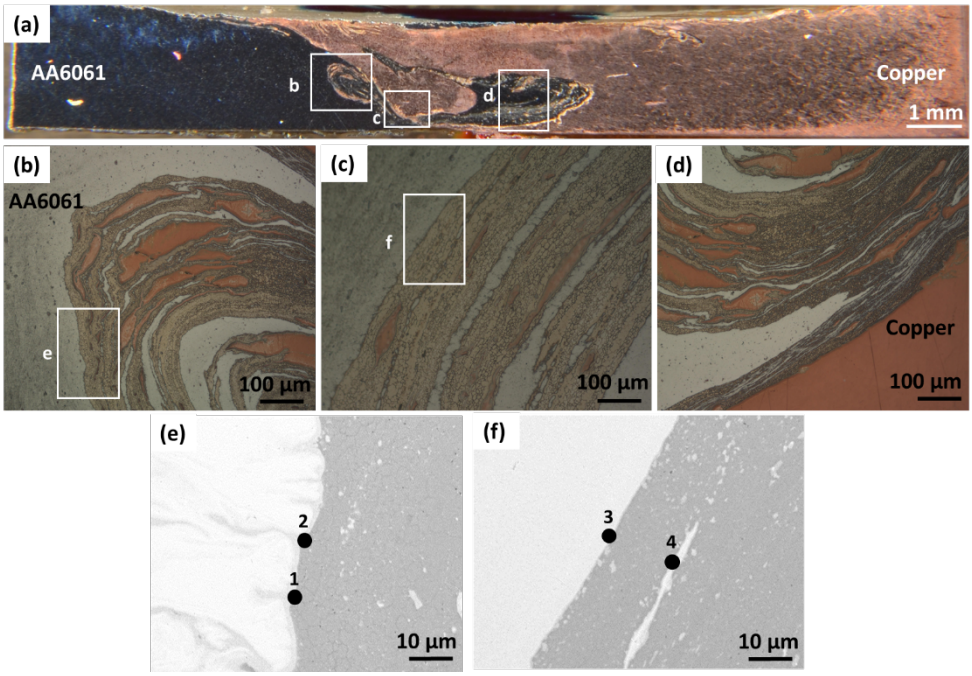

Fig. 10. (a) Typical cross-section of joint welded at 1400 rpm and 100 mm/min. (b) interface zone towards AA6061 side. (c) weld nugget. (d) interface zone towards copper side. (e) EDS points of rectangle e. (f) EDS points of rectangle f.

EDS analysis was performed at the interface zone to validate the developed approach of predicting the IMC formation (section 3.1). Figs. 10 (e) and (f), and Table 9 show that the newly generated layer close to the aluminium side is identified as AlCu according to the effective concentration of Al/Cu content (points 1 and 2). The possible IMC phases of points 3 and 4 are identified as Al_2Cu and Al_4Cu_9, respectively. This interface zone contains three different IMCs. The effective concentration of aluminium to copper under this non-equilibrium condition allows the AlCu phase to be formed first, i.e., lowest Gibbs free energy [2]. The Al_2Cu and Al_4Cu_9 phases formed later as a result of the diffusion kinetics, where the presence of these IMCs was determined further by XRD analysis.

Table 9

EDS results at weld nugget test no. 2 and 3

			Test no. 2			**Test no. 3**
Spectrum	Al at. %	Cu at. %	Probable Phase	Al at. %	Cu at. %	Probable Phase
1	53.18	46.82	AlCu	53.12	46.88	AlCu
2	55.60	44.40	AlCu	50.66	49.34	AlCu
3	62.62	37.38	Al_2Cu	71.70	28.30	Al_2Cu
4	35.22	64.78	Al_4Cu_9	37.72	62.28	Al_4Cu_9

Relatively small copper particles were observed as regularly distributed along the aluminium interfacial zone (Fig. 11 (a, b, & c)) of test no.3. Sufficient heat input generated by the relatively higher rotational speed of 1500 rpm is the reason behind this enhanced thermo-mechanical effect and the regular dispersion of copper particles in the aluminium. Towards the copper side, refined aluminium grains were intermixed with the copper particles, thus resulting in a wider copper thermomechanical affected zone (TMAZ) (Fig. 11 (d)).

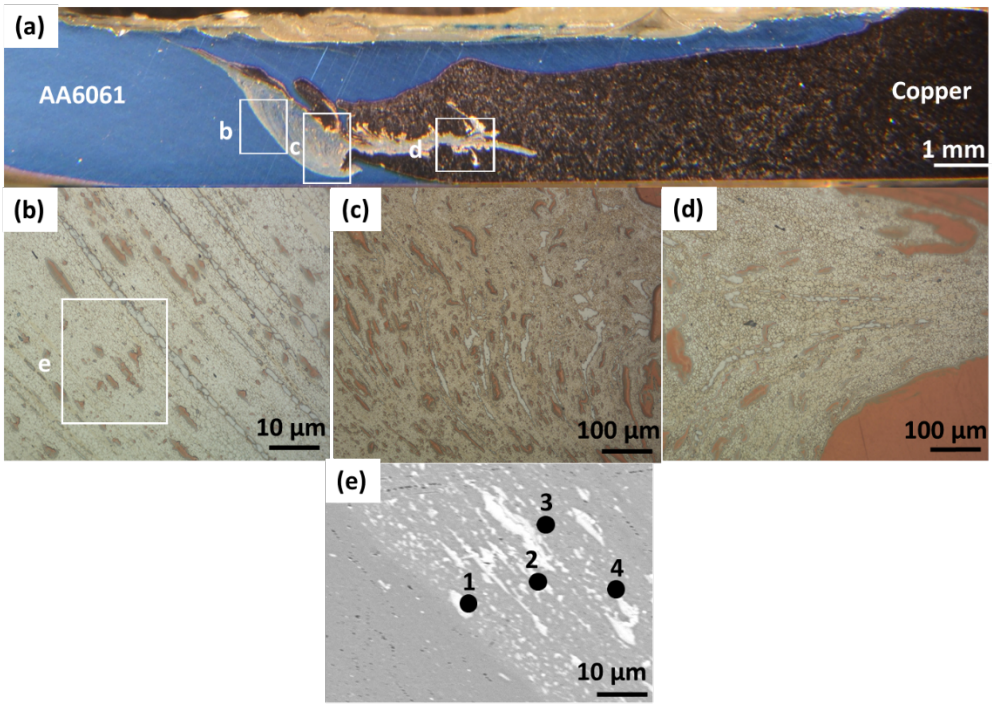

Fig. 11. (a) Typical cross-section of a joint welded at 1500 rpm and 100 mm/min. (b) interface zone towards the AA6061 side. (c) weld nugget. (d) interface zone towards the copper side. (e) EDS points of rectangle e.

According to the results of Table 9, points 1 and 2 in Fig. 11 (e), the AlCu IMC phase is identified close to the aluminium side. Al_2Cu and Al_4Cu_9 are the possible phases as per Fig. 11 (e) points 3-4, and Table 6. This is in agreement with the calculations presented in section 3.1 and supports the findings of test no.2.

3.3. Intermetallic phases at the weld nugget zone

XRD analysis was performed through the weld cross-sections to identify the phases present in the weld nugget. Fig. 12 presents the XRD patterns of the typical defect-free joints of test no. 2 and 3 of Table 6. It is confirmed that the dominant IMCs on the weld nugget of AA6061 and copper are AlCu, Al_2Cu and Al_4Cu_9. The presence of these IMCs agrees with findings discussed in section 3.1 however, the IMCs cannot be exclusively predicted on the basis of an Al-Cu phase diagram. The temperature during welding was calculated to be within the range of 0.8-0.9 of the aluminium melting temperature, i.e. exceeding the formation temperature of AlCu and Al_2Cu. However, in the case of Al_4Cu_9, the thermo-mechanical effect of FSW explains its formation at the weld nugget, where the melting temperature of this IMC, 1030°C, is higher than the peak temperature during FSW. This phenomenon has been reported

in different publications [3] and [5], as the thermo-mechanical action of the FSW tool promotes the formation of Al_4Cu_9 despite the lower temperature.

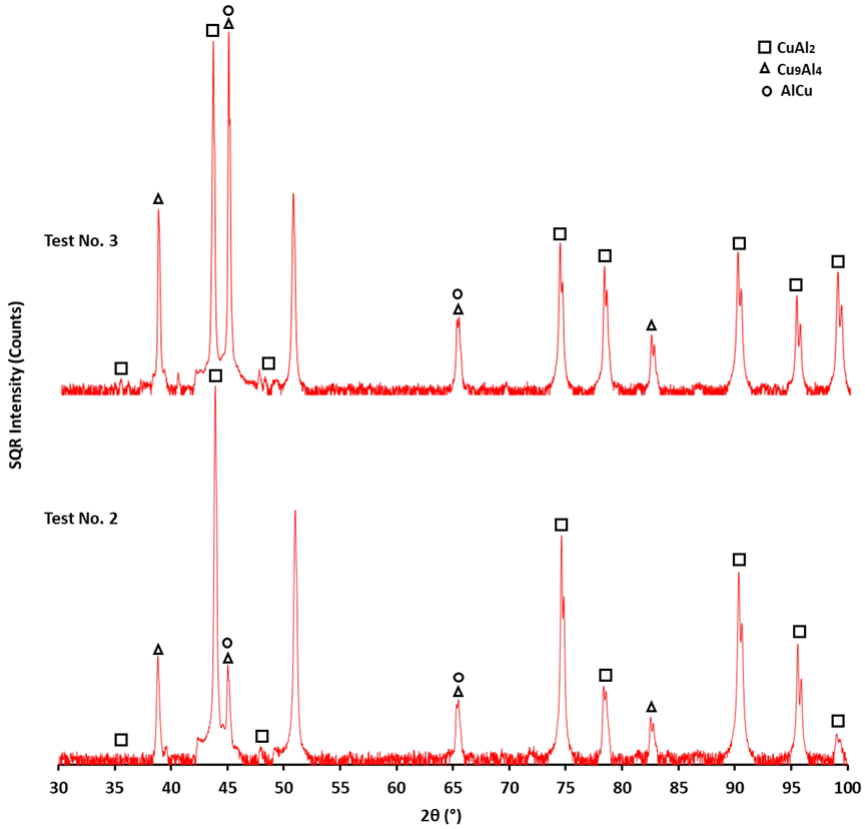

Fig. 12. XRD patterns acquired under tests no. 2 and 3.

The peak intensity increases by increasing the tool rotational speed. Qualitatively, it has been previously reported that high intensity peaks indicate higher IMC quantity [2]. Table 10 shows the results of quantifying the IMC volume fractions in the weld nugget considering the Topas Rietveld refinement method [26] on the XRD patterns of test no. 2 and 3. The developed method provides evidence of the increase in the IMCs volume as a result of increasing the tool rotational speed, where 1400 rpm and 1500 rpm are the tool rotational speeds of test no. 2 and 3, respectively.

Table 10

Quantitative analysis of the IMCs at different welding conditions (vol.%)

Test no.	Al_2Cu	AlCu	Al_4Cu_9
2	15.00	5.00	1.00
3	13.00	4.00	2.00

3.4. Joint mechanical strength

Fig. 13 (a) and (b) demonstrates the Vickers hardness measurements points together with the hardness distribution profiles of the dissimilar joints across and at the middle of the weld cross-section. It is observed that the hardness increases significantly at the SZ relative to the base metals. This is due to the presence of the IMCs which are hard and brittle in nature [1], accompanied with the formation of very fine recrystallised grains and copper-rich dispersed particles. Moreover, the combined effect of IMC formation and grain refinement due to recrystallisation increases the hardness at the TMAZ. The hardness variations are a direct result of the heterogeneous distribution of IMCs along with the softer materials (aluminium or copper) within the SZ.

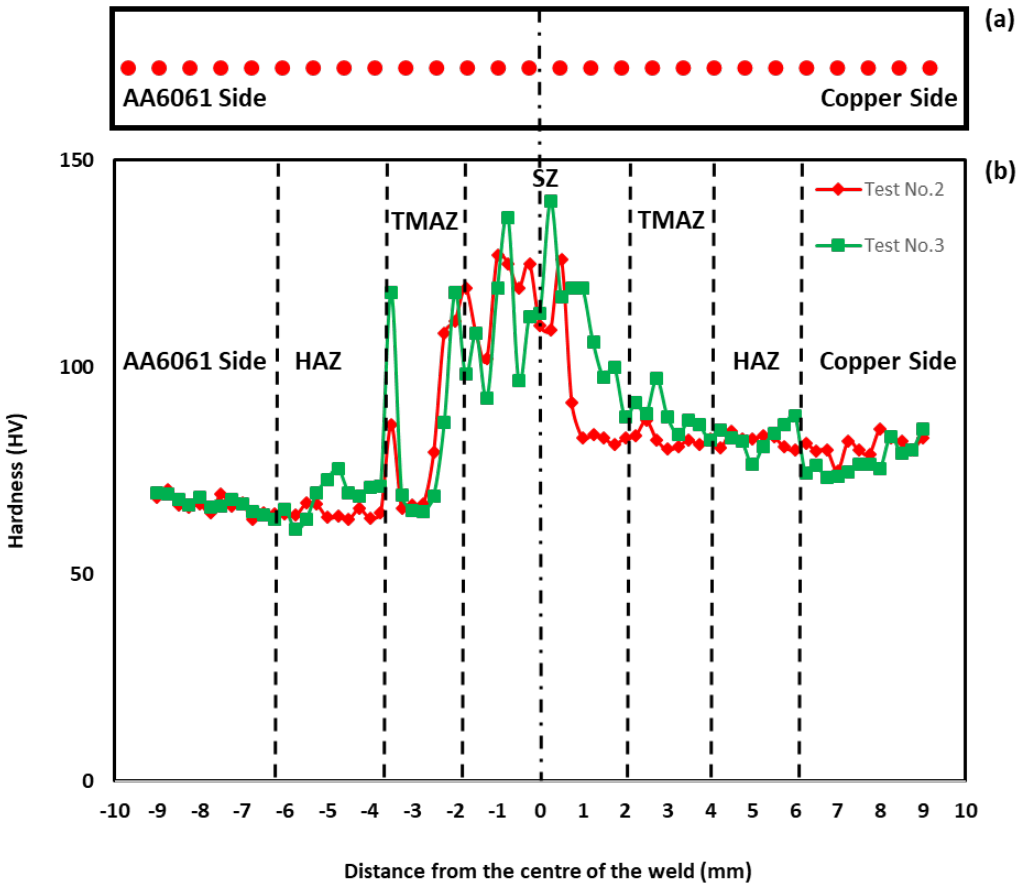

Fig. 13. (a) Vickers hardness measurement positions. (b) Vickers hardness distribution under tests no. 2 and 3.

The performance of the dissimilar joints has been evaluated by assessing their transverse tensile properties. Fig. 14 shows the yield strength, Young's modulus and joint efficiency of test no. 1, 2 and 3 (Table 6). It is revealed (Fig. 14) that increasing the heat input, by increasing the tool rotational speed from 1300 to 1500 rpm, improves the joint mechanical strength by approx. 7.0%. The increase in the tensile properties can be directly linked to the nature and quantity of IMCs. Additionally, this increase correlates to the evolved microstructure, where suitable material mixing is required to enhance the joint mechanical performance [1-2].

Unlike other published work [6-9] that placed the softer material on the RS, placing the AA6061 on the AS in this work resulted in a higher tensile strength of 194.5 MPa (92.0% joint efficiency). Further, FSWed joints at test no. 3 of higher tensile strength, experienced ductile fracture behaviour with different dimples sizes (Fig. 15). All the failures occurred at the TMAZ towards the AA6061 side.

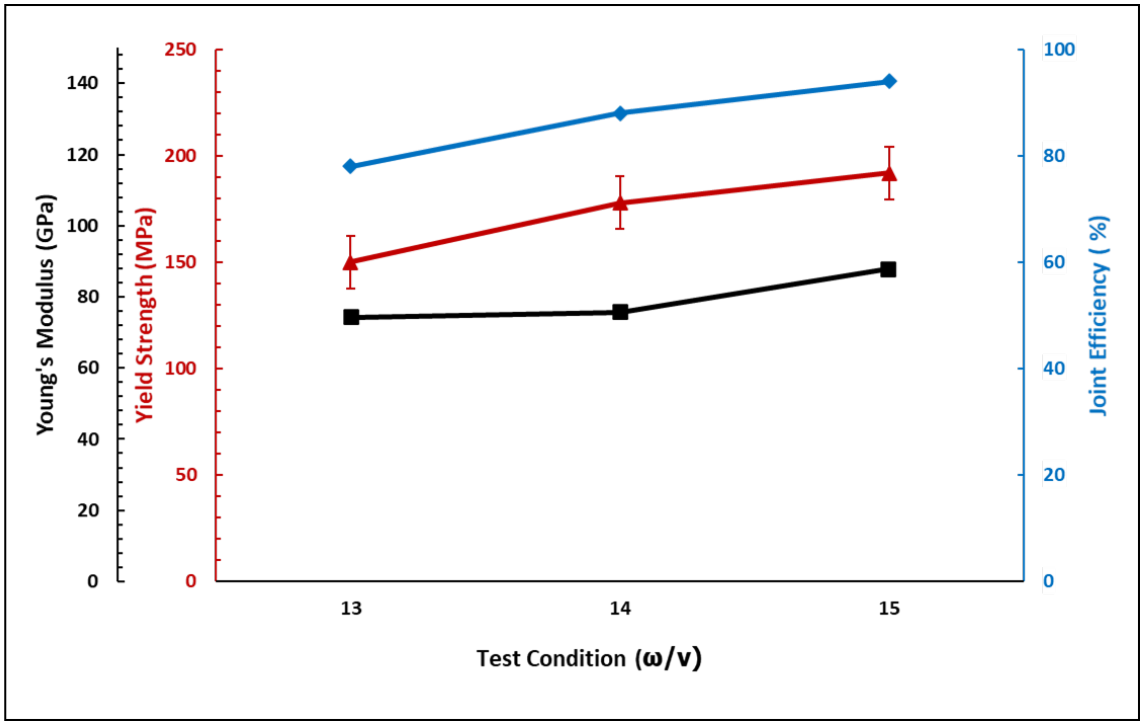

Fig. 14. Yield strength, Young's modulus, and joint efficiency at the different (ω/v) ratio.

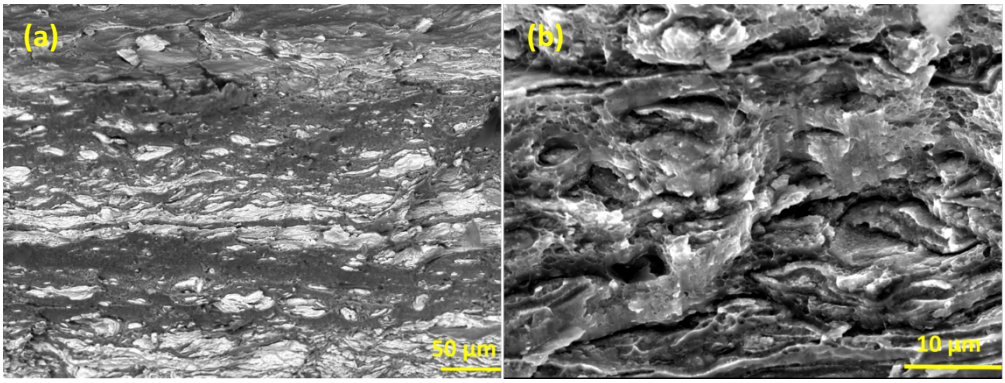

Fig. 15. SEM image of the fracture surface at weld test no. 3.

4. Conclusions

The FSW of AA6061 to commercially pure copper was investigated using experimental and numerical approaches, and the conditions that resulted in successful joints were identified. The following conclusions are drawn:

- The formation of IMCs in FSW of AA6061 to copper has been predicted and validated with the experimental results.

- The predominant intermetallic compounds in the aluminium-copper joint were AlCu, Al_2Cu and Al_4Cu_9.
- A successful weld joint between the two dissimilar materials has been achieved at 1400 rpm and 1500 rotational speeds and 100 mm/min traverse speed, where the softer material (AA6061) was placed at the advancing side without any tool offset.
- Improvements in the UTS were found to be controlled by the relatively regular distribution of IMCs together with the evolution of the composite like structure.

References

[1] N. Sharma, Z. A. Khan, and A. N. Siddiquee, “Friction stir welding of aluminum to copper—An overview”, The Transactions of Nonferrous Metals Society of China (English Ed., vol. 27, no. 10, pp. 2113–2136, 2017.

[2] I. Galvão, A. Loureiro & D. M. Rodrigues, “Critical review on friction stir welding of aluminium to copper”, Science and Technology of Welding and Joining, vol. 21, no. 7, pp. 523-546, 2016.

[3] Mishra , R.S., Ma, Z.Y, “Friction stir welding and processing”, Material Scince and Engineering: R: Reports, vol. 50, no. 1, pp.1–78, 2005.

[4] M. B. Uday, M. N. Ahmad Fauzi, H. Zuhailawati and A. B. Ismail, “Advances in friction welding process: a review”, Science and Technology of Welding and Joining, vol. 15, no. 7, pp. 534-558, 2010.

[5] N. Kumar, W. Yuan, and R. S. Mishra, “Introduction,” Friction Stir Welding of Dissimilar Alloys and Materials, A volume in Friction Stir Welding and Processing, pp. 1–13, 2015.

[6] Shailesh N. Pandyaa, Dr. Jyoti Menghani, “Optimum heat source position offset in welding of dissimilar Al-Cu metals using a theoretical approach”, Materials Today: Proceedings, vol. 5, pp. 26974–26980, 2018.

[7] J. Ouyang, E. Yarrapareddy, and R. Kovacevic, “Microstructural evolution in the friction stir welded 6061 aluminum alloy (T6-temper condition) to copper”, Journal of Materials Processing Technology, vol. 172, no. 1, pp. 110–122, 2006.

[8] I. Galvão, J. C. Oliveira, A. Loureiro and D. M. Rodrigues, "Formation and distribution of brittle structures in friction stir welding of aluminium and copper: influence of process parameters", Science and Technology of Welding and Joining, vol. 16, no. 8, pp. 681–689, 2011.

[9] C. Genevois, M. Girard, B. Huneau, X. Sauvage and G. Racineux, “Interfacial reaction during friction stir welding of Al and Cu”, Metallurgical and Materials Transactions A, vol. 42, no. 8, pp. 2290–2295, 2011.

[10] M.-N. Avettand-Fenoël, R. Taillard, G. Ji and D. Goran, “Multiscale study of interfacial intermetallic compounds in a dissimilar Al 6082-T6/Cu friction-stir weld”, Metallurgical and Materials Transactions A, vol. 43, no. 12, pp. 4655–4666, 2012.

[11] C. W. Tan, Z. G. Jiang, L. Q. Li, Y. B. Chen and X. Y. Chen, “Microstructural evolution and mechanical properties of dissimilar Al–Cu joints produced by friction stir welding”, Materials and Design, vol. 51, pp.466–473, 2013.

[12] P. Xue, D. R. Ni, D. Wang, B. L. Xiao, and Z. Y. Ma, “Effect of friction stir welding parameters on the microstructure and mechanical properties of the dissimilar Al–Cu joints”, Materials Science and Engineering: A, vol. 528, no. 13–14, pp. 4683–4689, 2011.

[13] H. J. Liu, J. J. Shen, L. Zhou, Y. Q. Zhao, C. Liu and L. Y. Kuang, “Microstructural characterisation and mechanical properties of friction stir welded joints of aluminium alloy to copper”, Science and Technology of Welding and Joining, vol. 16, no. 1, pp. 92–98, 2011.

[14] I. Galvão, R. M. Leal, D. M. Rodrigues, and A. Loureiro, “Influence of tool shoulder geometry on properties of friction stir welds in thin copper sheets”, Journal of Materials Processing Technology, vol. 213, pp. 129–135, 2013.

[15] A. A. Naumov, F. Y. Isupov, O. V Panchenko, and E. N. Rylkov, “Dissimilar Welding of Cu and Al Alloys by Friction Stir Welding and Impulse Friction Stir Welding”, Twenty-eighth International Ocean and Polar Engineering Conference, Japan, pp. 166–171, 2018.

[16] F. Al-Badour, N. Merah, A. Shuaib, and A. Bazoune, “Coupled Eulerian Lagrangian finite element modeling of friction stir welding processes”, Journal

of materials processing technology, vol. 213, no. 8, pp. 1433–1439, 2013.

[17] B. Meyghani, M. Awang, S. S. Emamian, M. K. Mohd Nor, and S. R. Pedapati, “A Comparison of Different Finite Element Methods in the Thermal Analysis of Friction Stir Welding (FSW)”, Metals (Basel)., vol. 7, no. 11, pp. 450, 2017.

[18] G. Buffa, J. Hua, R. Shivpuri, and L. Fratini, “A continuum based fem model for friction stir welding—model development”, Materials Science and Engineering: A, vol. 419, no. 1–2, pp. 389–396, 2006.

[19] X. He, F. Gu, and A. Ball, “A review of numerical analysis of friction stir welding,” Progress in Materials Science, vol. 65, pp. 1–66, 2014.

[20] G. R. J. William H.Cook, “A constitutive Model and Data for Materials Subjected to Large Strains, High Starin Rates and High Temperatures”, in Proceedings 7th International Symp. on Ballistics, 1983.

[21] H. W. Zhang and Z. Zhang, “A fully coupled thermo-mechanical model of friction stir welding”, International Journal of Advanced Manufacturing Technology, vol. 37, pp. 279–293, 2008.

[22] R. Nandan, G. G. Roy, T. J. Lienert, and T. Debroy, “Three-dimensional heat and material flow during friction stir welding of mild steel”, Acta Materialia, vol. 55, no. 3, pp. 883–895, 2007.

[23] V. Shokri, A. Sadeghi, and M. H. Sadeghi, “Thermo-mechanical modeling of friction stir welding in a Cu-DSS dissimilar joint”, Journal of Manufacturing Processes, vol. 31, pp. 46–55, 2018.

[24] ASTM E8 / E8M-21, Standard Test Methods for Tension Testing of Metallic Materials, ASTM International, West Conshohocken, PA, 2021.

[25] N. Ponweiser, C.L. Lengauer, and K.W. Richter:Intermetallics, vol. 19, pp. 1737–46, 2011.

[26] Kristin Husebo Hestnes, Bjorn Eske Sorensen, “Quantitative mineral characterisatization of granitic pegmatite using Topas Rietveld XRD refinement”, Proceedings of the 10th International Congress for Applied Mineralogy (ICAM), pp. 335-343, 2012.